

Dynamical renormalization of anharmonic lattices at the onset of fracture: Analytical results for scaling, noise, and memory

F. A. Oliveira*

International Centre of Condensed Matter Physics, Universidade de Brasilia, CP 04667, 70919-970 Brasilia DF, Brazil

(Received 28 September 1994; revised manuscript received 5 April 1995)

We present here results for dynamical renormalization of an anharmonic lattice. We investigate the dynamics of the lattice at the onset of fracture, and we show the existence of a map of this lattice into a transformed lattice with disorder (crack). By studying the properties of the transformed lattice we get exact analytical results for the decimation of the noise, and approximate analytical results for the dynamical scaling of the lattice and dynamical memory for the crack. We discuss the existence of a nonhydrodynamical behavior and how it affects the correlation between motions of adjacent particles. By drawing on the results of simulations and analytical methods, we are able to discuss how these concepts may be used to interpret more intensive simulations and experiments.

I. INTRODUCTION

The problem addressed in this paper is that of understanding the scaling properties of a classical lattice for which the interaction between the nearest neighbors is given by an anharmonic force. In a previous work¹ we reported extensive simulations in order to determine the conditions under which an anharmonic chain will break. There were two main conclusions from that study. First, in order for irreversible breaking to occur in a stretched chain, a bond must be extended to a length considerably greater than the length at which the restoring force is maximized. Second, the breaking rate of a bond may be expressed in terms of an attempt frequency and an Arrhenius factor. While the Arrhenius factor was satisfactorily described in terms of the height of an effective energy barrier, the attempt frequency was found to be orders of magnitude smaller than expected from a Kramers² type theory.

In the present paper we move a step closer in the direction of understanding the dynamics of the breaking. The approach that we shall take will be to follow the evolution of the lattices at the onset of fracture. In this way we focus our attention on the length of a single bond, and by drawing on simulations and reasonable hypotheses, we obtain analytical results for the noise decimation, scaling, correlation function, and, consequently, memory.

We shall find the rather surprising result that the correlation function for the motion of adjacent particles of an anharmonic stretched chain may be approximately described using the single-chain phonon spectrum, which can be expressed in a very simple form. We discuss how the scaling displays a nonhydrodynamical behavior and how that can be used to explain the discrepancy found in the long-time behavior.

Scaling methods are essential in circumstances where a system is scaling invariant or acts as if it were so.³ As a

general rule, whenever a characteristic control length diverges, as happens at any continuous phase transition, critical effects occur whose treatment requires scaling (renormalization group) methods,³⁻⁶ as far as the phenomena associated with the length are concerned, the system behaves as if it were scale invariant at the transition. In this way, scaling on linear lattices becomes a powerful and elegant tool, since these systems have a recursive hierarchical geometry such as fractals.⁷ Although linear dynamics is still very useful in the study of fractures, and a number of very useful results may be predicted from them⁸⁻¹¹ a nonlinear model is a necessity for a more realistic approach.^{1,12,13}

Nonlinear equations¹⁴ do not, in general have simple recursive hierarchical geometries. Consequently no general picture of scaling and dynamics has been presented for them, except in some particular situations. Some of these particular situations are found in continuous physical systems, such as growth phenomena at interfaces described, for example, by a KPZ (Kadar-Parisi-Zhang) equation.¹⁵ Continuous physical systems are described dynamically by partial differential equations or field theories. Thus they have infinitely many degrees of freedom, but can exhibit low-dimensional chaos, which has a fractal signature in itself.¹⁶ Such continuous systems have the shortcoming that they have no explicit reference to the structure of the crystal lattice. However, the fact that such a simple, continuous, and in some cases linear approach is able to produce such remarkable and sometimes surprising results leads us to the conclusion that some *general mechanisms must characterize those structures at the onset of a fracture*. The main purpose of this work is to make explicit some of those mechanisms; in particular, we prove that an anharmonic chain at the onset of fracture may be seen as a harmonic one with a defect. We present here results for dynamical scaling in a nonlinear lattice. Our starting point is that at the

onset of fracture the formation of a fractal pattern, i.e., the existence of a recursive hierarchical geometry, implies that the lattice can be renormalized. In Sec. II we state the lattice dynamics, from which we get the scaling properties of the noise in Sec. III, and the properties of memory in Sec. IV. The existence of the hierarchical relations Eqs. (15), (12), and (13) exhibits the main aspects of the dynamical lattice normalization.

II. CHAIN DYNAMICS

Consider a one-dimensional lattice of N particles of mass M , which interact with their neighbors via an anharmonic interaction F . The chain has initial length $L = Na$, where a is the lattice spacing. We stretch the chain, and the new length becomes $L = N(a + S)$. The generalized Langevin equation for the l th particle is then

$$M\ddot{x}_l = F(a + S + x_l - x_{l-1}) - F(a + S + x_{l+1} - x_l) - M \int_0^t \gamma(t-t')\dot{x}_l(t')dt' + h_l(t). \quad (1)$$

Here x_l is the displacement from the equilibrium position, $h_l(t)$ describes the interaction with a thermal reservoir at temperature T , and it is connected with the memory $\gamma(t)$ via the fluctuation dissipation theorem. In the simulations to be described in this paper we use periodic boundary conditions, and the force F is obtained from a Lennard-Jones potential

$$U(x) = \epsilon \left[\left(\frac{a}{x} \right)^{12} - \left(\frac{a}{x} \right)^6 \right], \quad (2)$$

with unit ($\epsilon = 1$) binding energy. However, the main conclusions are the same for fractures of other nonlinear systems. We focus our analysis on the evolution of the distance between two consecutive displacements $y_l = x_{l+1} - x_l$. From Eq. (1) we get an equation of the motion for y_l ,

$$M\ddot{y}_l = -F(a + S + y_{l-1}) + 2F(a + S + y_l) - F(a + S + y_{l+1}) - M \int_0^t \gamma(t-t')\dot{y}_l(t')dt' + [h_{l+1}(t) - h_l(t)]. \quad (3)$$

Length is in units of a , and time in units of $\tau_S = 2\pi/\omega_S$, where ω_S is the maximum phonon frequency of the stretched lattice. We verify that breaking occurs at a single bond by recording as a function of time the instantaneously largest value of y_l (upper curve in Fig. 1). We see that at some point one particular bond starts to lengthen from the noise and increases inexorably to the vicinity of a saturation value given by the distance between the broken ends of the relaxed chain. The lower

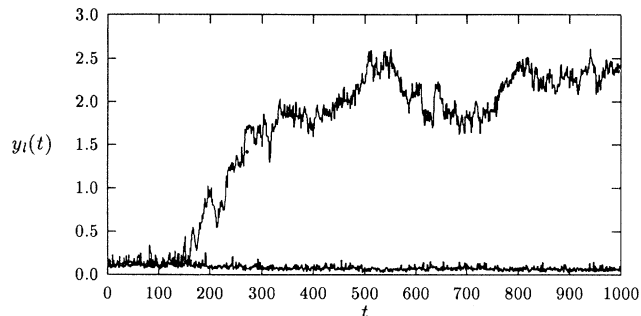


FIG. 1. The evolution of a breaking process in a chain. We plot as a function of time the instantaneously largest value of $y_l = x_{l+1} - x_l$. The lower curve depicts the second-largest y_l . The chain is composed of 100 particles interacting via a Lennard-Jones potential. Distances are given in units of the lattice parameter of the unstretched chain a , and time in units of $\tau_S = 2\pi\omega_S^{-1}$, with ω_S as the maximum phonon frequency of the chain. Here $S = 0.03$, $T=0.05$, $\gamma(t) = 2\gamma_0 \delta(t)$, and $\gamma_0 = 0.25\omega_0$.

curve (Fig. 1) depicts the second-largest y_l , and shows that no other bond has experienced any significant extension during the breaking process. Figure 2 shows the position j in the lattice where this maximum occurs. It shows that j fluctuates initially and finally stabilizes at a given position ($j = 16$). That corresponds to a situation where the system is just starting a real break, and where $y_l \ll y_j$ for $l \neq j$. The average of an ensemble of 800 chains shows that most of the time the system is in that metastable situation. Consequently for all $y_l \ll y_j$ the variations are just of the same order as harmonic fluctuations.

A very simple effective potential for a chain with a single breaking bond may be obtained as

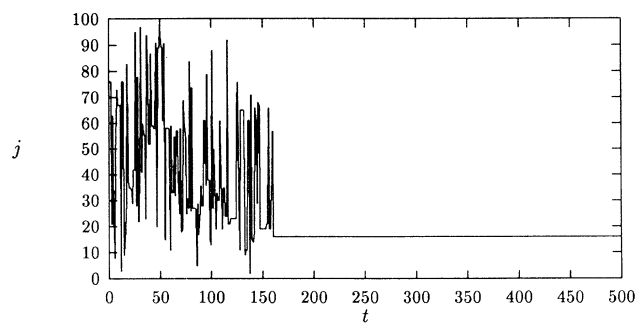


FIG. 2. The position j in the lattice where a maximum y_j occurs. For the first maximum (upper curve in Fig. 1) it localizes at $j = 16$. For the second maximum, not showed here, it continues fluctuating from point to point in the lattice.

$$U_{\text{eff}}(y) = U(a + S + y) + (N - 1)U\left(a + S - \frac{y}{N - 1}\right). \quad (4)$$

This potential corresponds to a situation where the stretched bond assumes a value y and all the other $N - 1$ bonds relax by an amount $-y(N - 1)^{-1}$, in such a way that the length of the lattice remains fixed. From this potential we obtain the effective force

$$F_{\text{eff}}(y) = F(a + S + y) - F\left(a + S - \frac{y}{N - 1}\right). \quad (5)$$

The term $-y(N - 1)^{-1}$ takes into consideration the finite size of the chain and certainly becomes infinitesimal for long chains. As $N \rightarrow \infty$ the second term on the right-hand side (RHS) of Eq. (5) is just the zero-temperature stress in the chain. Consequently $F_{\text{eff}}(y)$ can be seen as the competition between the stress that pulls off the particle and the bond restoring force.

In Fig. 3 we plot $U_{\text{eff}}(y)$ as a function of y for $N = 100$ and two different strains: $S = 0.014$ (curve *a*) and $S = 0.019$ (curve *b*). This potential has two minima, one at $y = 0$ and another at $\tilde{y} = (N - 1)S$. For small S (Fig. 3, curve *a*), when the internal elastic energy is smaller than the energy necessary to break a bond, the system will not break in an irreversible way. For $S = 0.019$, the unbroken position $y = 0$ corresponds to a metastable situation while the large \tilde{y} will be an absolute minimum. Consequently, given enough time the particle will move from a metastable situation to a stable one, or, correspondingly, the chain will break. In the later situation there is a barrier E_b to overcome, which is less than the bond energy ϵ . The height of the barrier E_b is a function of the strain S [for example, $E_b(S = 0.03) \approx 0.18$]; consequently, as one increases S , E_b decreases and breaking becomes easier.

The breaking of two bonds will need an extra energy $\epsilon = 1.0$; consequently the probability of two breaks will be $\exp(-\beta\epsilon)$ smaller than that of one break. In our simulation $\beta\epsilon = 20$, but in real life situations this number can be larger (for a polyethylene bond at room temperatures $\beta\epsilon \approx 150$).

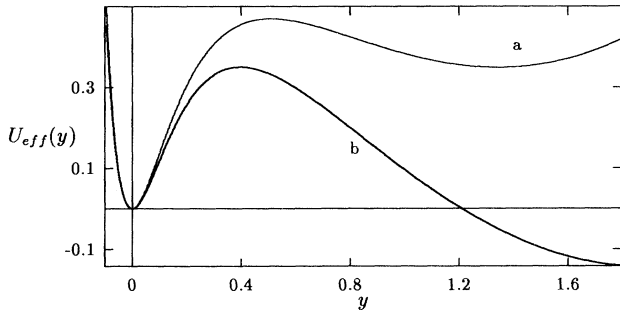


FIG. 3. The effective potential for a break of a bond as a function of the bond elongation. This potential corresponds to a minimum energy necessary to break a bond. $S = 0.014$ (curve *a*) and $S = 0.019$ (curve *b*).

III. SCALING AND NOISE

From the last section we may say that the break will occur in just one bond, and all of the other bonds will undergo small oscillations. With this very important information in mind, we introduce, in Eq. (3), $y_j = y$ and $y_{l \neq j} = \phi_l - y(N - 1)^{-1}$ ($\sum_l \phi_l = 0$ with $\phi_j = 0$), and then expand Eq. (3) in small powers of ϕ_l to obtain

$$\mu \ddot{y} = F_{\text{eff}}(y) - \mu \int_0^t \Gamma(t - t') \dot{y}(t') dt' + g_j(t) \quad \text{for } l = j \quad (6)$$

and

$$M \ddot{\phi}_l = K(S)(\phi_{l+1} - 2\phi_l + \phi_{l-1}) - F_{\text{eff}}(y)\delta_{l,j \pm 1} - M \int_0^t \gamma(t - t') \dot{\phi}_l(t') dt' + g_l(t) \quad \text{for } l \neq j. \quad (7)$$

Here $K(S)$ is the strain-dependent force constant of the chain, $\mu = M/2$. The new noises $g_l(t)$ are given by

$$g_l(t) = f(t)\delta_{l,j} + (1 - \frac{1}{2}\delta_{l,j})[h_{l+1}(t) - h_l(t)], \quad (8)$$

where $f(t)$ is the coherent part of the noise given by

$$f(t) = \frac{1}{2}K(S)[\phi_{l+1}(t) - 2\phi_l(t) + \phi_{l-1}(t)]. \quad (9)$$

Equation (9) shows clearly that $f(t)$ is a very correlated noise. The fluctuation dissipation theorem requires

$$\langle g_l(t)g_l(t') \rangle = \begin{cases} \mu k_B T \Gamma(t - t') & \text{for } l = j, \\ M k_B T \gamma(t - t') & \text{for } l \neq j. \end{cases} \quad (10)$$

Equations (6)–(10) show some marvelous simple aspects of breaking; Eq. (6) shows a particle of effective mass $\mu = M/2$ moving in a effective potential which carries the nonlinearity, and is coupled through the noise to a harmonic chain, Eq. (7). The chain went through a quite remarkable transformation; it has changed from an anharmonic chain with periodic boundary conditions to a harmonic one with fixed ends at $l = j$ ($\phi_j = 0$). We shall call the linear chain of Eq. (7) the *transformed lattice*. Notice that the *particle transformed memory* $\Gamma(t)$, which is modulated by the noise of harmonic oscillators, becomes quite different from the function $\gamma(t)$ of the chain.

To start our scaling procedure we move to points of the chain far from the end and rewrite Eq. (7) as

$$-\Omega \phi_l = \phi_{l-1} - 2\phi_l + \phi_{l+1} + g_l(t), \quad (11)$$

with $\Omega = MK(S)^{-1}\omega^2$; ω is the vibrational frequency of a given mode. For simplicity we leave the discussion of memory for the next section. We eliminate the sites $l - 1$ and $l + 1$ to get

$$-\Omega' \phi_l = \phi_{l-2} - 2\phi_l + \phi_{l+2} + g'_l(t), \quad (12)$$

where $\Omega' = 4\Omega(\Omega - 1)$ and $g'_l = g_{l+1} - 2g_l + g_{l-1} + \Omega g_l$. For successive iterations we have

$$\Omega_n = 4\Omega_{n-1}(1 - \Omega_{n-1}), \quad (13)$$

n being the order of iteration. It is a well-known result that Eq. (13) produces a chaotic map in the region $0 < \Omega < 1$, with density¹⁴ $P(\Omega) \propto [\Omega(1 - \Omega)]^{-1/2}$. This distribution has a very high probability for numbers close to zero; consequently we may drop the term Ωg_l in subsequent iterations, and the density distributions for g'_l may be built up from the distributions for $g_l - g_{l+1}$. For example, consider first a discrete noise $g_j = \Theta m$, with Θ as the intensity and $m = 0, \pm 1$. The initial probability W_0 has the value $W_0(m) = 1/3$, while for the first iteration (first decimalization) the results will be $W_1(\pm 2) = 1/9$, $W_1(\pm 1) = 2/9$, $W_1(0) = 1/3$. The interval has been doubled and the probability has been modified. After n decimalizations the probability may be written in the recursive form

$$W_n(k) = \sum_j W_{n-1}(j)W_{n-1}(k-j), \quad n \geq 1. \quad (14)$$

For large n ($n=5$ or 6), $W_n(k)$ has a binomial-type distribution. The binomial distribution does not obey simple scaling;¹⁷ rather it is steady multifractal, as discussed by Kadanoff¹⁸ in the context of the avalanche model. Notwithstanding this multifractal aspect, we show that in the continuous limit, the renormalization approach, implicit in Eq. (14), drives the noise distribution towards equilibrium.

In order to obtain the density of probability, or the density distribution, of noise at the iteration n , $P_n(x)$, we first localize x in discrete intervals k . We define now $W_n(k)$ as the probability of order n of finding x in a given interval k . Now, in the continuous limit we obtain

$$P_n(x) = \int_{a_n}^{b_n} P_{n-1}(x')P_{n-1}(x-x')dx', \quad n \geq 1, \quad (15)$$

where $P_n(x)$ is the density distribution of noise at iteration n . Here $|x| < L_n$ and $L_n = 2L_{n-1}$. From this condition we get $a_n = (-L_n - x + |x|)/2$, $b_n = (L_n - x - |x|)/2$. Notice that the distribution for g'_l will be $P_2(x)$. The recurrence relation defined by Eq. (15) has very important properties. For an even starting distribution, all the subsequent distributions will be even; the distributions will be decreasing functions of $|x|$, with vanishing values for $|x| \geq L_n$; finally, as $n \rightarrow \infty$, the probability becomes a Gaussian, independent of the initial $P_0(x)$. The information about the local P_0 fades away when the collective effects of the lattice ($n \rightarrow \infty$) drive the noise distribution toward equilibrium. Actually, with only a few iterations, the distribution becomes very close to a Gaussian. For example, using our white noise distribution $P_0(x) = 1/2$ for $|x| < 1$ we get

$$P_1(x) = \frac{1}{4}(2 - |x|), \quad |x| < 2, \quad (16)$$

and

$$P_2(x) = \begin{cases} (32 - 12x^2 + 3|x|^3)/96, & 0 < |x| < 2, \\ (4 - |x|)^3/96, & 2 < |x| < 4. \end{cases} \quad (17)$$

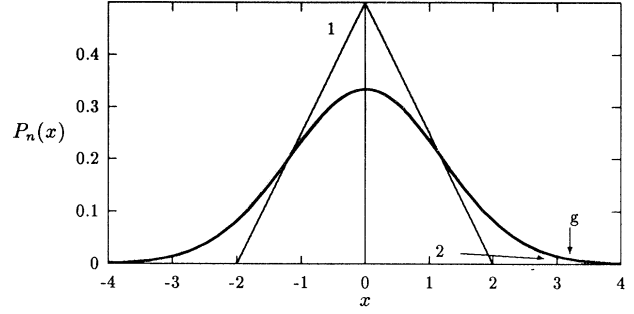


FIG. 4. Density of probability $P_n(x)$ of finding the noise within the value Θx and $\Theta(x + dx)$ as a function of x . Here x is a random number $-L_n \leq x \leq L_n$, $L_n = 2L_{n-1}$, n is the order of iteration, and Θ is a measure of the intensity of the noise. $P_n(x)$ is obtained iteratively from $P_{n-1}(x)$. We start with the white noise distribution $P_0(x) = 1/2$ and $L_0 = 1$. We plot (1) $P_1(x)$ and (2) $P_2(x)$ and the Gaussian (g) $P(x) = \exp(-\pi x^2/9)/3$. The Gaussian has the same height as P_2 , and is normalized to unity.

In Fig. 4 we plot $P_n(x)$ as a function of x : (1) P_1 given by Eq. (16) and (2) P_2 given by Eq. (17). As a reference we plot (g) the Gaussian $P(x) = \exp(-\pi x^2/9)/3$, which has the same height as P_2 . For $n > 2$ the form of $P_n(x)$ becomes quite complicated, but it can always be obtained numerically by use of Eq. (15). However, it may not be necessary, since, as one can see in Fig. 4, $P_2(x)$ fits a Gaussian surprisingly very well. The recursive form of Eq. (15) is so constraining that any even starting distribution is expected to become close to a Gaussian after a few iterations. The fact that the noise distribution tends toward a Gaussian is by itself a remarkable result, since one should bear in mind that in this new picture (effective particle + transformed lattice) the particle is in a nonequilibrium situation. This result is very useful as well from the computational point of view, since we may apply locally any available distribution $W_0(n)$, or $P_0(x)$, and the renormalization procedure of the noise distribution [Eq. (15)] will give us assurance that the lattice noise distribution will be in a thermal equilibrium, even under certain extreme conditions such as fracture.

IV. SCALING, FRACTONS, AND MEMORY

We now turn to the central theoretical problem of the dynamics of breaking in an anharmonic lattice: *What can our theory can say about correlation of motions in adjacent particles, memory, and scaling at the onset of fracture?* Such ingredients are necessary for one to be able of make predictions that may be checked by simulations or real experiments. Of course no analytical theory capable of accounting for all the richness of the problem is available at present, and so we try to develop a simple picture of the phenomena as a stepping stone to a more complete theoretical explanation. Our first step is to ob-

serve that from Eq. (10) the memory can be expressed formally as

$$\Gamma(t) = \gamma(t) + \frac{\omega_S^2}{2} R(t), \quad (18)$$

where

$$R(t) = \frac{M\omega_S^2}{8k_B T} \sum_{l=j\pm 1} \langle \phi_l(t)\phi_l(0) \rangle. \quad (19)$$

Here $\langle \rangle$ refers to an ensemble average. This equation shows that since more “friction” is added to the system from the coherent modes, even a starting white noise $\gamma(t) = 2\gamma_0\delta(t)$ will introduce some memory into the system.

For simple monoatomic harmonic chains, that is, those whose spectra are phonons of wave number q and angular frequency $\omega(q) = \omega_S \sin(qa/2)$, the correlation function $\langle x_l(t)x_l(0) \rangle$ has been intensively investigated (see Ref. 27 and references therein). Florencio and Lee²⁷ point out that the divergence in the mean square displacement $\langle x_l(0)^2 \rangle$ was a consequence of the periodic boundary condition. For a chain with fixed ends, their result is finite, but depends on the lattice site l . Following their procedure we get

$$R(t) = \frac{2}{\pi} \int_0^{\pi/2} \cos[\omega_S t \sin(y)] dy. \quad (20)$$

The integral was obtained by making the q space continuous. In frequency space Eq. (20) may be written in a most suitable form as

$$R(t) = \int_0^{\omega_S} \rho(\omega) \cos(\omega t) d\omega. \quad (21)$$

The last equation will be generalized for a nonhydrodynamical regime [see Eq. (28)]. Using $\rho(\omega) = 2/\pi\sqrt{\omega_S^2 - \omega^2}$ we get

$$R(t) = J_0(\omega_S t); \quad (22)$$

here J_0 is a Bessel function. Since our ϕ_l is the difference between two amplitudes, the correlation function $R(t)$ is neither divergent nor site dependent. This result is surprisingly simple, compared with the long series obtained²⁷ for the function $\langle x_l(t)x_l(0) \rangle$. For the simulations, we define

$$R_s(t) = M\omega_S^2(4k_B T)^{-1} \overline{\phi_{j\pm 1}(t)\phi_{j\pm 1}(0)}, \quad (23)$$

where

$$\overline{\phi_{j\pm 1}(t)\phi_{j\pm 1}(0)} = \frac{1}{\tilde{\tau}} \int_0^{\tilde{\tau}} \phi_{j\pm 1}(t+t')\phi_{j\pm 1}(t') dt'. \quad (24)$$

In Fig. 5 we plot $R(t)$ as a function of time, for the same conditions as those in Figs. 1 and 2. Curve a of Fig. 5 is the result from Eq. (22), while curve b is the result of a full numerical simulation of the anharmonic lattice [Eqs. (1) and (24)]. In the simulation we use $\tilde{\tau} = 20\,000$ time step intervals. For $t = 0$, Eq. (19) predicts $R(0) = 1$, while our simulation gives $R_s(0) = 1.016$. For the region $t < \tau_S/2$, the agreement is remarkable. This provides

strong support for the concept of a linear chain with fixed ends. For $t > \tau_S/2$ curve b is displaced from curve a , and shows some kind of interference phenomenon.

Before we proceed with a more detailed analysis of the modes, we are led to the question of stability: *How stable are those modes since even a small nonlinearity may result in instabilities?* Unfortunately, this is not a fully answerable question given the state of art of our theory. However, we shall mention here that the strong (exact) variational principle present in the effective potential (4) yields a hidden variational principle for the equation of motion. Consequently the system will follow the minimum action path (geodesy) leading to a break, and we may say that the equations of motion [Eqs. (6) and (7)] represent that minimum action principle. We can refer to the experiments of Fig. (5) as a good test for that claim. A very important fact here is that curve b of Fig. 5 does not display an exponential decay, but rather, as curve a , a $t^{-1/2}$ decay. We notice as well that even for very long times ($\omega_S t \approx 20\pi$) the amplitude is almost the same as that of curve a . This strongly suggests that the difference between them is not due to anharmonic corrections, which would induce instability in the modes and an exponential decay envelope. Simulations with harmonic chains show a similar behavior. Notice that the equivalence between Eqs. (19) and (23), namely, the ergodic theorem, is itself a proof, within the limitation of our simulation, that the lattice is not very far away from equilibrium as we discussed in the previous section.

To examine this manifestation further we look at the low-frequency modes, which have the main responsibility for the long-time behavior. To drive the system to large y , we initially need some higher modes, such as solitons; once this result is achieved, the linearization of the lattice shows that the low modes, the most coherent ones, are mainly responsible for continuing the breaking dynamics. As a consequence, we may claim that the self-similarity of the *transformed lattice* may be used to understand the

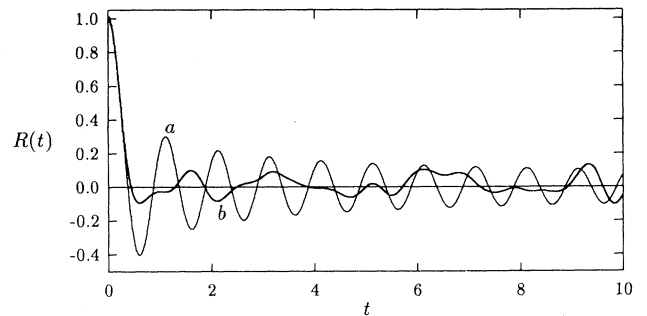


FIG. 5. The correlation function $R(t)$ as a function of time. Parameters as in Fig. 1. We start to count the time t when the maximum localizes. Curve a displays the theoretical value for the harmonic chain $J_0(\omega_S t)$, obtained from the full spectrum of the one-dimensional phonons, with the hydrodynamical behavior ($\omega \propto k$) in the long-wavelength limit. Curve b is the full simulation from the anharmonic chain. We use 20 000 time steps; no normalization was done. For large t (small ω) curve b suggests a nonhydrodynamical behavior.

fractal characteristic of the anharmonic one. The effect of disorder can be incorporated in the same way as it was for linear phonons¹⁹ or for a spin glass with a low concentration p of impurities.²⁰ In the presence of impurities the new maps are

$$p_{n+1} = p_n(2 - p_n), \quad (25)$$

$$\Omega_{n+1} = f(\Omega_n, p_n), \quad (26)$$

where p_n and Ω_n are the concentration and the frequency at the iteration of order n . For zero impurity concentration ($p = 0$), Eq. (26) reduces to Eq. (13). The precise form of f need not be specified here, since the result for the linear chain is well known.^{14,20} The important aspect is that the frequency spectrum and the bifurcation diagram are that of a linear lattice. In this way we have achieved the dynamical renormalization of the anharmonic lattice. Notice that this result does not depend on the particular form of the force F .

Equation (25) can be extended to dimension $d > 1$. The new equation (besides the trivial fixed points $p = p^* = 0, 1$) may have one critical $p^* = p_c$, $0 < p_c < 1$, which allows a percolation transition. Consequently a fracture process for $d=2,3$ can be seen as a percolation transition. The general form of Eq. (26) may be difficult to get except in few cases. The important point is that the lattice dynamics is the same for different systems with a similar geometry; in this way the renormalization for phonons¹⁹ is the same as that of magnons ($\omega \propto k$) in dilute Heisenberg chains^{20,21} and in the quantum XY model.²² For $d = 1$, Stinchcombe²⁰ obtained Eq. (26) explicitly, which combined with Eq. (25) yields for the low modes $\Omega_{n+1} \propto \lambda \Omega_n$ [$\lambda = \lambda(p^*)$], and Ω scales as $a^{2\alpha}$, which gives $\omega \propto \Omega^{1/2} \propto k^\alpha$. For a general d , those results can be obtained from the scaling hypothesis²³

$$\omega = k^\alpha G(\xi k), \quad (27)$$

with ξ as the characteristic length of the random geometry for both limits $\xi k \ll 1$, and $\xi k \gg 1$ $G(\xi k)$ has a power law form. Consequently those results provide $\omega \propto k^\alpha$. Here, α is expressed as a function of the critical exponents. Harris and Stinchcombe²¹ obtained the dynamical critical exponents exactly for a dimension d . From their results we know that for $\xi k < 1$ we have $\alpha = 1$, while $\xi k > 1$ yields a nonhydrodynamical ($\alpha \neq 1$) behavior. Those modes have been named fractons. Experimental results from inelastic neutron scattering²⁴⁻²⁶ are in agreement with the theory, and they show the hydrodynamical-fracton crossover for $\xi \approx k^{-1}$.

The fracton modes will induce modifications in the density of states, affecting consequently almost all physical quantities. For given α we generalize Eq. (21) to obtain

$$R(t) = \int_0^{\omega_S} \rho_\alpha(\omega) \cos(\omega t) d\omega; \quad (28)$$

here k is related to ω via Eq. (27). The density of states $\rho_\alpha(\omega)$, and consequently the memory, is strongly affected

by the fractal dimension of the lattice. For a few values of α , Eq. (28) can be integrated in terms of elementary functions, but numerical integration can be carried out in general if we know $\rho_\alpha(\omega)$.

For $\xi k_D \leq 1$, Eq. (22) is the proper result for $R(t)$. For $\xi k \geq 1$ and $\alpha \neq 1$ we have a crossover in the dispersion relation, making the evaluation of Eq. (28) more difficult. This crossover separates the hydrodynamical region, where the waves are underdamped and not localized, from the region where the waves are localized and overdamped (fractons). Unfortunately there is no result for the full spectrum, which is necessary for the evaluation of the integral in Eq. (28). The difference between the hydrodynamical and the fracton modes may explain the difference between curves a and b of Fig. 5. The localization of those waves may explain as well the results of Fig. 2, where the large y stays in a localized metastable position until it evolves irreversibly to a break. There cannot be an explanation within the framework of a hydrodynamical theory.

The evolution of a particle through a barrier has been the object of intensive investigation in the last 50 years, and represents a very active area of physics and chemistry known as reaction rate theory.^{2,28-30} The characteristic time for a particle to go through a barrier (such as that in Fig. 3) will depend on the Laplace transform of its memory $\tilde{\Gamma}(z)$ and of its derivative $d\tilde{\Gamma}(z)/dz$ for values of z close to zero (long-time behavior). To get a estimate of $\tilde{\Gamma}(z)$ for $z \ll \omega_S$, we suppose that the harmonic-type correlation will hold as well for $\alpha \neq 1$. The Laplace transform of $R(t)$ yields

$$\tilde{R}(z) = \int_0^{\omega_S} \frac{d\omega \rho_\alpha(\omega) z}{\omega^2 + z^2}, \quad (29)$$

which for $z \approx 0$ becomes $\tilde{R}(z) \approx \pi \rho_\alpha(z)/2$. Notice that for $z = 0$ and $\alpha = 1$ this agrees with the exact $\tilde{R}(z) = 1/\sqrt{\omega_S^2 + z^2}$ result. For the low fracton modes $\rho_\alpha(\omega) \propto (\omega/\omega_S)^\eta$, with $\eta = \frac{1}{\alpha} - 1 < 0$; consequently we expect that the nonhydrodynamical regime will produce values for $\tilde{R}(z)$ larger than the hydrodynamical one.

In Fig. 6 we plot $\tilde{R}(z)$ as a function of z . The function $\tilde{R}(z)$ is given in units of $1/\omega_S$, while z is given in units of ω_S . Curves a and b of Fig. 6 are the Laplace transforms of curves a and b of Fig. 5, respectively. For large z (short times) we see that curve b of Fig. 6 converges to curve a of Fig. 6. For small z the effects of the low modes are appreciable. From the results of simulation and analytical methods, Eq. (29), one may be able to say that the nonhydrodynamical behavior induces a higher density of states for the low modes than a hydrodynamical regime.

The change of memory and the presence of a nonhydrodynamical behavior can be related to the large healing capacity of a bond and consequently to the long breaking time found in some simulations.¹ These times are 300 times longer than those obtained from estimates which do not consider the dynamical effect of the memory. This healing capacity is also observed experimentally¹³ in iron whiskers under stress. They contain few defects and remain undamaged in a metastable state until a fracture

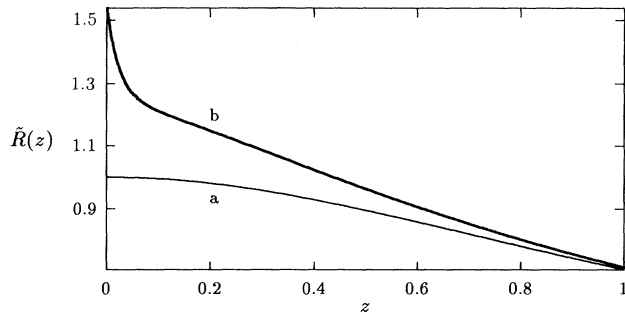


FIG. 6. The Laplace transform of the correlation function $\tilde{R}(z)$ as a function of z . $\tilde{R}(z)$ is in units of $1/\omega_S$ and z in units of ω_S . Curves *a* and *b* are the Laplace transforms of curves *a* and *b* of Fig. 5, respectively. For larger z ($z \approx \omega_S$) the curves converge to the same value. The large values of $\tilde{R}(z \ll \omega_S)$ in curve *b*, correspond to a higher density for the nonhydrodynamical modes.

occurs. This phenomenon was labeled *delayed fracture*.¹³ The *dynamical memory* and the *transformed lattice* may be useful to explain those phenomena, both qualitatively and quantitatively.

V. CONCLUSION

In conclusion, by analysis of the evolution of a break in an anharmonic lattice, we map this lattice into a *transformed lattice* which is a linear one with a defect. This lattice can be renormalized, and that represents a dynamical renormalization of a nonlinear lattice. Comparison between the analytical results and simulations suggest that the main modes are those of a harmonic lattice. The short-time behavior of $R(t)$ shows that no higher modes such as solitons are present in an appreciable manner. The lattice defect or crack can be viewed as one particle moving in an effective potential subjected to a noise composed of two parts: one due to the thermodynamical bath and the other due to the motions of neighbor particles, which gives an origin to a *transformed dynamical memory*. We obtain a formal expression for the transformed

memory, which can be easily evaluated for a small correlation length ξ . A first estimate shows that the inclusion of the nonhydrodynamical regime may affect the analysis of data from experiments and simulations. The memory can be used to obtain a closed analytical expression for the breaking rate of long chains. That would be a very important result since the state of art is only for a particle moving in an effective potential.^{29,30} However, before we proceed to more detailed calculations, we need more precise information about the crossover region and the fractons. The full theory goes beyond the objective of this work, but the results present here are part of the effort of building up such theory. We expect to treat these problems in a self-consistent way in a subsequent publication.³¹

For $d > 1$ the concentration of cracks p and its diversity of size and shape are a function of the temperature, strain, and history of the lattice, which point toward nonuniversal values for α . Notwithstanding the fact that the situation is quite different from the one-dimensional case, the presence of cracks may still induce relaxation of the other bonds and a harmonic behavior. That the low modes are the most important ones in driving the system toward a break may explain why some harmonic approximations are not so bad at all. Additional simulations and analytical results are necessary to further explore the concept of *the transformed lattice* in higher dimensions. However, we hope that the concepts developed here will be a stepping stone toward a more complete analytical theory of fracture in low-dimensional systems, and in particular, we expect that the renormalization procedure discussed here may be applied in different areas of physics.

ACKNOWLEDGMENTS

I would like to acknowledge the kind hospitality of Professor Philip Taylor at the Physics department of CWRU and Dr. Timothy P. Doerr and Professor Robin Stinchcombe for very important discussions. This work was supported by CNPq and FINEP (Brazil).

* Electronic address: fao@iccmp.br

¹ F. A. Oliveira and P. L. Taylor, J. Chem. Phys. **101**, 10118 (1994); F. A. Oliveira, Mod. Phys. Lett. B **9**, 31 (1995).

² H. A. Kramers, Physica **7**, 284 (1950).

³ L. P. Kadanoff, Physics **2**, 263 (1966).

⁴ K. G. Wilson, Phys. Rev. Lett. **28**, 584 (1972).

⁵ K. G. Wilson and M. E. Fisher, Phys. Rev. Lett. **28**, 240 (1972).

⁶ For a review in scaling dynamics see R. B. Stinchcombe, in *Current Trends in Condensed Matter Physics*, edited by A. Ferraz, F. A. Oliveira, and R. Osorio (World Scientific, Singapore, 1990).

⁷ B. Mandelbrot, *The Fractal Geometry of Nature* (Freeman, San Francisco, 1982).

⁸ L. de Arcangelis and H. J. Herrmann, Phys. Rev. B **39**, 2678 (1989).

⁹ W. C. Curtin and H. Scher, Phys. Rev. Lett. **67**, 2457 (1991).

¹⁰ H. J. Herrmann, Physica D **38**, 192 (1989); in *Random Fluctuations and Pattern Growth*, edited by H. E. Stanley and N. Ostrowsky (Kluwer, Dordrecht, 1988).

¹¹ T. P. Doerr and P. L. Taylor, J. Chem. Phys. **101**, 10107 (1994).

¹² R. B. L. Selinger, R. M. Lynden Bell, and W. M. Gelbert, J. Chem. Phys. **98**, 9809 (1993).

¹³ S. S. Brenner, J. Appl. Phys. **33**, 11 (1962); *Fiber Composite Materials* (American Society for Metals, Metals Park, OH, 1965).

¹⁴ E. Infeld and G. Rowlands, *Nonlinear Waves, Solitons and Chaos* (Cambridge University Press, Cambridge, England, 1990).

¹⁵ M. Kadar, G. Parisi, and Y. C. Zhang, Phys. Rev. Lett.

- 56**, 889 (1986).
- ¹⁶ J. P. Eckmann and I. Proracia, in *Nonlinear Physical Phenomena*, edited by A. Ferraz, F. A. Oliveira, and R. Osorio (World Scientific, Singapore, 1991).
- ¹⁷ P. Billings, *Ergodic Theory and Information* (Wiley, New York, 1965), p. 139.
- ¹⁸ L. P. Kadanoff, *Physica D* **38**, 213 (1989).
- ¹⁹ R. Orbach, in *Scaling Phenomena in Disorder Systems*, edited by R. Pynn and A. Skjeltorp (Plenum Press, New York, 1985); *Physica D* **38**, 266 (1989); A. Aharony, S. Alexander, Ora Entin-Wohlman, and R. Orbach, *Phys. Rev. Lett.* **58**, 132 (1987).
- ²⁰ R. Stinchcombe, *Phys. Rev. Lett.* **50**, 200 (1983).
- ²¹ K. J. Harris and R. Stinchcombe, *Phys. Rev. Lett.* **50**, 1399 (1983).
- ²² A. C. Maggs, L. L. Gongalves, and R. B. Stinchcombe, *J. Phys. A* **19**, 1927 (1986).
- ²³ B. I. Halpenin and P. C. Hohenberg, *Phys. Rev.* **177**, 952 (1969).
- ²⁴ J. P. Boucher, C. Dupas, W. J. Fitzgerald, K. Knorr, and J. P. Renard, *J. Phys. (Paris)* **39**, L86 (1978).
- ²⁵ Y. Endoh, G. Shirane, R. Birgeneau, and Y. Ajiro, *Phys. Rev. B* **19**, 1476 (1979).
- ²⁶ Y. J. Uenrura and R. J. Borgeneau, *Phys. Rev. B* **36**, 1024 (1987).
- ²⁷ J. Florencio and M. H. Lee, *Phys. Rev. A* **30**, 3231 (1985).
- ²⁸ For a recent review see P. Hänggi, P. Talkner, and M. Borkovec, *Rev. Mod. Phys.* **62**, 251 (1990).
- ²⁹ E. Pollack, S. C. Tucker, and B. J. Berne, *Phys. Rev. Lett.* **65**, 1399 (1990).
- ³⁰ Surgit Singh and G. W. Robinson, *Chem. Phys.* **183**, 365 (1994).
- ³¹ F. A. Oliveira (unpublished).